Two-Dimensional Mass Spectrometry for Proteomics, a Comparative Study with Cytochrome c

Maria A. van Agthoven,[||] Christopher A. Wootton,[||] Lionel Chiron,[⊥] Marie-Aude Coutouly,[§,¶] Andrew Soulby,[||] Juan Wei,[||] Mark P. Barrow,[||] Marc-André Delsuc,[‡,⊥] Christian Rolando,[†] and Peter B. O'Connor*,[||]

[||]Department of Chemistry, University of Warwick, Gibbet Hill Road, CV4 7AL Coventry, West Midlands, United Kingdom

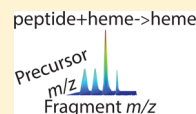[⊥]CASC4DE, Le Lodge, 20, av. du Neuhof, 67100 Strasbourg, France

[§]NMRTEC, Bld. Sébastien Brandt, Bioparc - Bat. B, 67400 Illkirch-Graffenstaden, France

[‡]Institut de Génétique et de Biologie Moléculaire et Cellulaire, INSERM, U596; CNRS, UMR7104; Université de Strasbourg, 1 rue Laurent Fries, 67404 Illkirch-Graffenstaden, France

[†]Université de Lille, CNRS, USR 3290, MSAP, Miniaturisation pour la Synthèse l'Analyse et la Protéomique, FR 3688, FRABIO, Biochimie Structurale & Fonctionnelle des Assemblages Biomoléculaires, and FR 2638, Institut Eugène-Michel Chevreul, F-59000 Lille, France

S *Supporting Information*

ABSTRACT: Two-dimensional Fourier transform ion cyclotron resonance mass spectrometry (2D FT-ICR MS) allows the correlation between precursor and fragment ions in tandem mass spectrometry without the need to isolate the precursor ion beforehand. 2D FT-ICR MS has been optimized as a data-independent method for the structural analysis of compounds in complex samples. Data processing methods and denoising algorithms have been developed to use it as an analytical tool. In the present study, the capabilities of 2D FT-ICR MS are explored with a tryptic digest of cytochrome c with both ECD and IRMPD as fragmentation modes. The 2D mass spectra showed useful fragmentation patterns of peptides over a dynamic range of almost 400. By using a quadratic calibration, fragment ion peaks could be successfully assigned. The correlation between precursor and fragment ions in the 2D mass spectra was more accurate than in MS/MS spectra after quadrupole isolation, due to the limitations of quadrupole isolation. The use of the second dimension allowed for successful fragment assignment from precursors that were separated by only m/z 0.0156. The resulting cleavage coverage of cytochrome c almost matched data provided by high-resolution FT-ICR MS/MS analysis, but the 2D FT-ICR MS method required only one experimental scan.

Fourier transform ion cyclotron resonance mass spectrometry (FT-ICR MS) is a well-described mass spectrometry technique relying on the cyclotron motion of ions in a high magnetic field.[1,2] The pulse sequence for two-dimensional FT-ICR MS (2D FT-ICR MS) was first proposed by Pfändler et al.[3] and was inspired in part by NOESY NMR spectroscopy[4] and in part by an experiment on ion de-excitation by Marshall et al.[5] The principle of 2D FT-ICR MS has been explained in previous studies[6,7] and can be found in the Supporting Information.

The first 2D FT-ICR experiments were performed by Pfändler et al. with ion–molecule reactions[8] and IRMPD[9] as fragmentation modes. Another pulse sequence called stored waveform ion radius modulation (SWIM) was tested and applied by Ross et al.[10] and by van der Rest and Marshall.[11] However, due to limitations in computer capacities, 2D FT-ICR MS was not pursued further. In 2010, the first 2D FT-ICR MS was obtained on a commercial mass spectrometer with IRMPD[12] and later ECD[13] as fragmentation modes. Subsequently, a data processing and visualization program was developed[14] along with denoising algorithms to reduce the effect of scintillation noise.[15,16] In order to optimize signal-to-noise ratios, the pulse sequence was optimized.[17] With an

atmospheric pressure photoionization source, 2D FT-ICR MS was recently shown to easily differentiate the fragmentation pathways of radical and protonated cholesterol species with a m/z difference of 1 Da, which would have been difficult by typical means of ion isolation.[18]

2D FT-ICR MS has been shown to be a fast and data-independent analytical method to get the fragmentation patterns of the ions from a given sample and can now be applied to samples of increasing complexity, such as the tryptic digests of proteins. In this study, we analyze the tryptic digest of cytochrome c by use of 2D FT-ICR MS with ECD and IRMPD as fragmentation modes. The tryptic digest of cytochrome c (104 residues, 12.3 kDa) is a well-known standard used in the development of many methods in bottom-up proteomics, from peptide maps[19] and H/D exchanges[20] to affinity-based mass spectrometry with magnetic iron oxide particles.[21] The present study shows the performance of 2D FT-ICR MS with a cytochrome c digest and compares it to standard MS/MS studies.
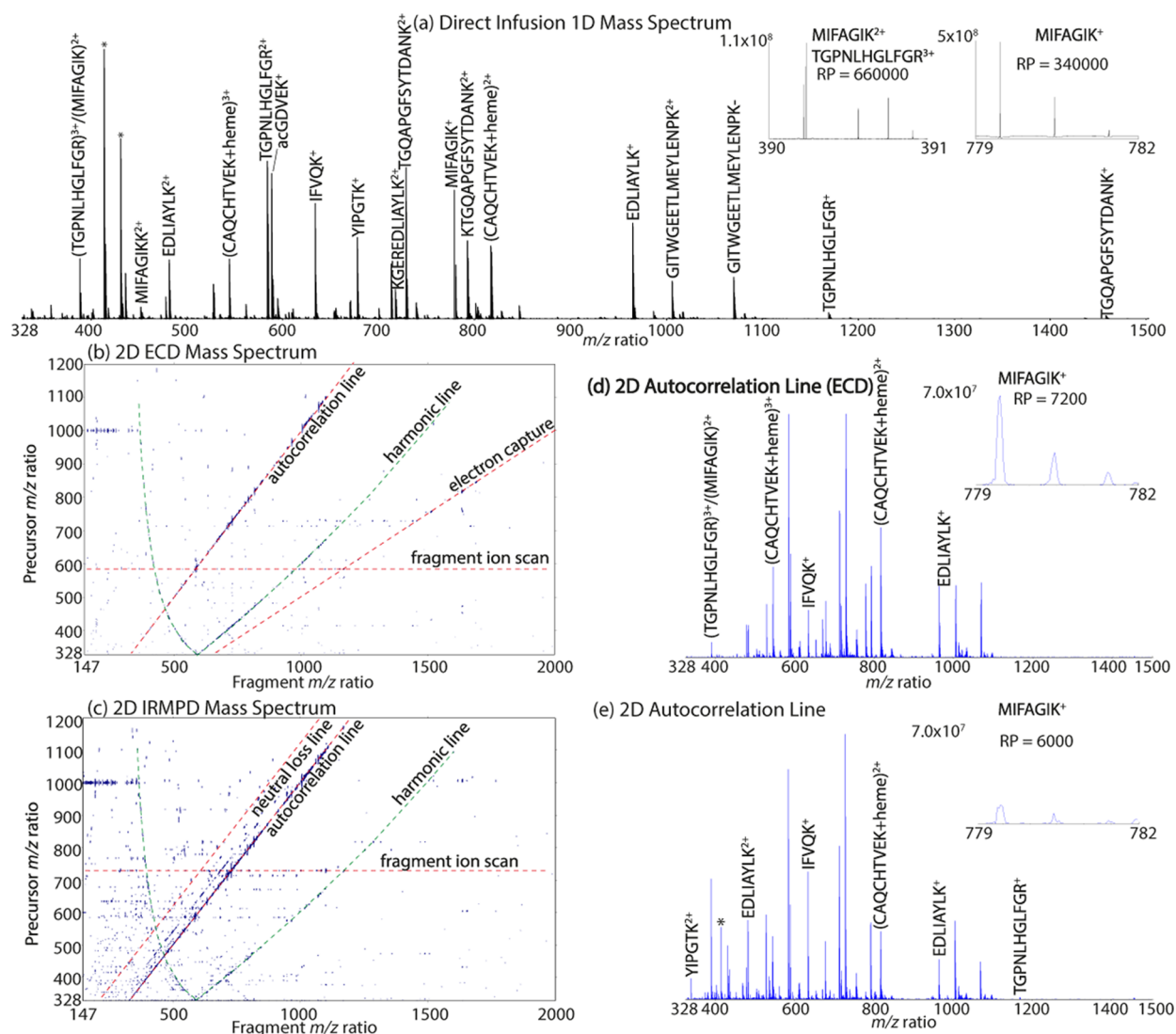
Figure 1. (a) Mass spectrum of the tryptic digest of cytochrome c (insets: zoom on the peak of MIFAGIK^{2+} and TGPNLHGLFR^{3+} at m/z 390, zoom on the peak of MIFAGIK^{+} at m/z 779). (b) Two-dimensional mass spectrum of the tryptic digest of cytochrome c with ECD as a fragmentation mode. (c) Two-dimensional mass spectrum of the tryptic digest of cytochrome c with IRMPD as a fragmentation mode. Red lines highlight the autocorrelation line and other characteristic lines in 2D mass spectra. Green lines highlight 2D artifacts produced by higher harmonic frequency modulation during t_1 and folded in the m/z representation. (d) Autocorrelation line of the 2D mass spectrum of cytochrome c with ECD as a fragmentation mode (inset: zoom on autocorrelation peak of MIFAGIK^{+} at m/z 779). (e) Autocorrelation line of the 2D mass spectrum of cytochrome c with IRMPD as a fragmentation mode (inset: zoom on autocorrelation peak of MIFAGIK^{+} at m/z 779).

EXPERIMENTAL METHODS

Sample Preparation. Bovine cytochrome c tryptic digest (lyophilized) was purchased from Thermo Scientific (Amsterdam, The Netherlands). A stock solution of 8 pmol/μL was obtained with 95% water that was deionized using a Direct-Q 3 Ultrapure Water System (Millipore, Nottingham, United Kingdom) and 4.9% acetonitrile (VWR International Ltd., Lutterworth, United Kingdom) with 0.1% formic acid (Sigma-Aldrich, Dorset, United Kingdom) and was stored at −18 °C. From this, a sample of 800 fmol/μL was prepared with 90% deionized water, 9.8% acetonitrile, and 0.2% formic acid.

Instrument Setup. All experiments were performed on a 12T solariX Fourier transform ion cyclotron resonance mass spectrometer (Bruker Daltonik, GmbH, Bremen, Germany). The sample was ionized using a home-built nanoelectrospray (nESI) ion source at a rate of 7−8 μL/hour. After transfer through two octopoles and a quadrupole, ions are accumulated

in a hexapole-based collision cell for 0.1 s and transferred through a transfer hexapole (1.0 ms transfer period) to the Infinity Cell for fragmentation and detection.[22]

Control MS and MS/MS Data. The control MS spectrum was measured with 4 Mwords (16 bits) transient length (1.6777 s) over a mass range of m/z 147.4−1500 (1250−122.8 kHz frequency range), with a pulse at 15% excitation power (70 V$_{pp}$) and 20 μs per frequency in 1804 decrements of 625 Hz. The spectrum was accumulated for 50 scans.

All control MS/MS data were recorded for 50 scans with 4 Mwords (16 bits) transient length (1.6777 s) over a mass range of m/z 147.4−3000 (1250−61.4 kHz frequency range), with a pulse at 15% excitation power (70 V$_{pp}$) and 20 μs per frequency in 1902 decrements of 625 Hz. ECD was performed using electrons from a 1.5 A indirectly heated hollow cathode dispenser.[23] IRMPD was performed using a Synrad 48-2 CO$_2$ laser (25 W) with a 10.6 μm wavelength at 50% power

(Mukilteo, WA, United States). Experimental conditions particular to each MS/MS data are listed in Table S1 for ECD MS/MS data and in Table S2 for IRMPD MS/MS data.

2D Mass Spectra. The pulse sequence for the 2D FT-ICR MS experiment is presented in Scheme S1a. The excitation pulse P_1 and the encoding pule P_2 were identical, using a 15% excitation power (70 V_{pp} amplitude). In the ECD experiment, P_1 and P_2 had 4.0 μs per frequency. In the IRMPD experiment, P_1 and P_2 had 0.4 μs per frequency. The resulting frequency range in both experiments was 1250−61.4 kHz (1902 decrements of 625 Hz), resulting in a mass range of m/z 147.4−3000. The encoding delay t_1 was incremented by 1 μs 2048 times after an initial delay of 1 μs (Nyquist frequency: 500 kHz, mass range in the vertical precursor dimension: m/z 368.2−3000). The excitation pulse P_3 was set in both experiments at 15% excitation power (70 V_{pp} amplitude) with 20 μs per frequency with 1902 decrements of 625 Hz. Each transient was measured using 128k data points over a fragment mass range of m/z 147.4−3000 (frequency range of 1250−61.4 kHz). Each transient lasted 0.0262 s. The total acquisition time for each experiment was approximately 20 min. Each 2D mass spectrum had 2048 × 128k points, i.e. 256 M points.

In the 2D FT-ICR ECD MS experiment, the extraction lens was set at 60 V, the ECD bias was set at 2.1 V, and the irradiation period was 0.1 s. In the 2D IRMPD FT-ICR MS experiment, the laser power was set at 50%, and the irradiation period was 0.2 s.

Data Processing. The one-dimensional MS spectrum without fragmentation was phase-corrected with the Autophaser 6.0 phase correction software.[24−28] All one-dimensional spectra were first externally calibrated[29,30] with the solariXcontrol software (Bruker Daltonics, Billerica, MA, United States) using Agilent ESI-L Low Concentration Tuning Mix (Agilent Technologies, Stockport, United Kingdom) and then internally calibrated using known theoretical mass-to-charge ratios of the peptide ions in the cytochrome c tryptic digest with a quadratic calibration equation within the Data Analysis 4.0 software (Bruker Daltonik, GmbH, Bremen, Germany).

The 2D mass spectra were processed using the SPIKE software developed independently by the University of Strasbourg and CASC4DE (Illkirch-Graffenstaden, France)[14] in 64-bit Python programming language on a commercial platform distributed by Anaconda Continuum Analytics (Austin, TX, United States). Processed datafiles were saved using the HDF5 file format.

In the precursor ion dimension, the signals were digitally demodulated by using a time-dependent phase-rotation as a function of t_1. In the Bruker waveform generator, the oscillator is set at a frequency (ω_0) corresponding to the highest m/z ratio in the mass range. In 2D experiments, this means that the phase difference between the ion motion and the excitation voltage in the second pulse (P_2) is proportional to ($\omega_{ICR}+\omega_0$) × t_1 instead of $\omega_{ICR} \times t_1$. The digital demodulation is a linear phase correction along the vertical axis with a ω_0 frequency in order to remove the modulation of the signal according to the cyclotron frequency of the highest m/z ratio in the mass range.

Denoising was accomplished using the urQRd algorithm with a urQRd rank of 3.[16] The resulting 2D mass spectra were displayed in magnitude mode. Frequencies were converted in mass-to-charge ratios using Francl's equation with parameters from the external calibration for a MS spectrum.[31] The same calibration parameters were used in the precursor and the fragment dimension. Further internal calibration was conducted

on the horizontal fragment ion scans using a quadratic equation.[32]

RESULTS AND DISCUSSION

Figure 1a shows the one-dimensional control mass spectrum obtained from a long transient (4 Mwords and 1.67 s) processed with phase correction. The resulting resolving power at m/z 400 is 600,000. The internal calibration of the mass spectrum with the peptides assigned in the test chromatogram provided by the supplier (see Table S3 in the Supporting Information) allows the assignment of compounds with a high mass accuracy (0.29 ppm average absolute value of the mass accuracy). All of the peaks that were assigned to the tryptic digest of cytochrome c are listed in Table S4 of the Supporting Information (23 assigned peptides). To compare the efficiency of a 2D MS proteomics experiment and a standard MS/MS analysis, ECD and IRMPD were also applied on each of the peptides listed in Table S4 (Tables S1 and S2).

One-Dimensional FT-ICR MS of the Cytochrome c Digest. One of the peptides identified in the test chromatogram is MH_3^{3+} of IFVQKCAQCHTVEK (m/z 545.2784). This assignment is also found in several research articles with low-resolution mass analyzers.[33,34] A study of equine cytochrome c by Russell et al.[35] with a MALDI-TOF mass spectrometer found that the singly charged state of the same species could be assigned to [CAQCHTVEK+heme]$^+$ with sufficient mass accuracy (3 ppm). Henderson et al.[36] compared the measured collisional cross section of the ion at m/z 545.2 in ion mobility with the calculated collisional cross sections of both MH_3^{3+} of IFVQKCAQCHTVEK and MH_2^{3+} of [CAQCHTVEK+heme] and assigned the peak to MH_2^{3+} of [CAQCHTVEK+heme]. In Figure 1a, the most high-magnitude peak of this triply charged ion is measured at m/z 545.2095, with a mass accuracy of −0.15 ppm for and assignment of MH_2^{3+} of [CAQCHTVEK+heme], which agrees with this assignment. At m/z 390.2, the peptide identified in the test chromatogram is MH_3^{3+} of TGPNLHGLFGR. However, the peaks at m/z 390 in the mass spectrum show two overlapping isotopic distributions (see inset on the right side of Figure 1a): MH_3^{3+} of TGPNLHGLFGR at m/z 390.2122 (−0.10 ppm) and MH_2^{2+} of MIFAGIK at m/z 390.2278 (−0.11 ppm).

Three high-abundance singly charged contaminants are present in the mass spectrum at m/z 415.2115, m/z 432.2379, and m/z 437.1935. Because of the high resolution and mass accuracy of the mass spectrum, identifying the elemental compositions of these ions is possible: m/z 415.2115 can be assigned as $C_{24}H_{31}O_6^+$ (theoretically m/z 415.211515, with a mass accuracy of −0.04 ppm), m/z 432.2379 can be assigned as $C_{24}H_{34}NO_6^+$ (theoretically m/z 432.238064, with a mass accuracy of −0.38 ppm), and m/z 437.1935 can be assigned as $C_{24}H_{30}O_6Na^+$ (theoretically m/z 437.193460, with a mass accuracy of 0.23 ppm). Further investigation in the structure of these contaminants is in the Supporting Information (Figure S2, Tables S8 and S9).

2D ECD/IRMPD FT-ICR MS Proteomics on the Cytochrome c Digest. The denoised 2D mass spectra with ECD and IRMPD are shown in Figures 1b and 1c. On both 2D mass spectra, the autocorrelation line has been highlighted, as well as a horizontal fragment ion scan. In Figure 1b, an electron capture line can be seen for the capture of one electron by doubly charged ions. In Figure 1c, several neutral loss lines can be seen for IRMPD fragmentation: most of them correspond to water loss and ammonia loss from the doubly and triply
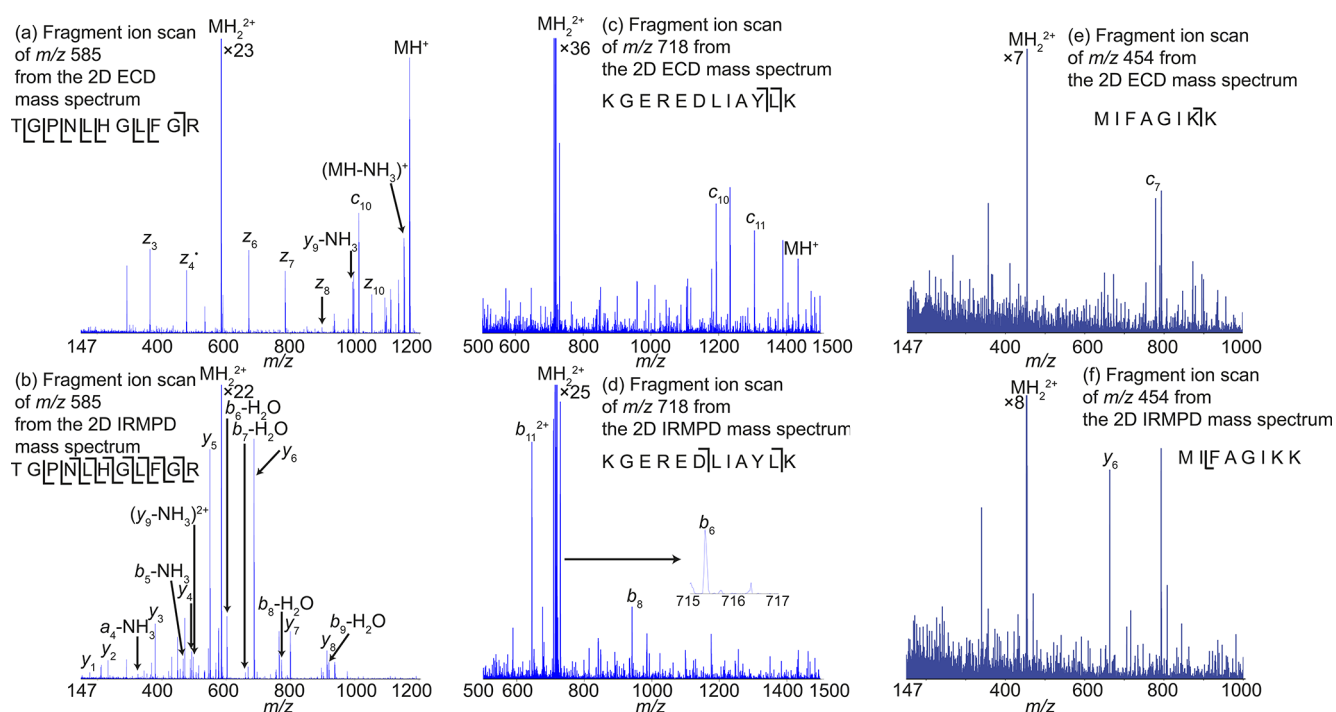
(a) Fragment ion scan of m/z 585 from the 2D ECD mass spectrum
T G P N L H G L F G R

MH_2^{2+} ×23
MH^+
$(MH-NH_3)^+$
c_{10}
z_3 $z_4^\cdot$ z_6 z_7 y_9-NH_3 z_8 z_{10}

147 400 600 800 1000 1200
m/z

(b) Fragment ion scan of m/z 585 from the 2D IRMPD mass spectrum
T G P N L H G L F G R

MH_2^{2+} ×22
b_6-H_2O
b_7-H_2O
y_5
y_6
$(y_9-NH_3)^{2+}$
b_5-NH_3
y_4
a_4-NH_3
y_3
y_1 y_2
b_8-H_2O
y_7
b_9-H_2O
y_8

147 400 600 800 1000 1200
m/z

(c) Fragment ion scan of m/z 718 from the 2D ECD mass spectrum
K G E R E D L I A Y L K

MH_2^{2+} ×36
c_{10}
c_{11}
MH^+

500 600 800 1000 1200 1400 1500
m/z

(d) Fragment ion scan of m/z 718 from the 2D IRMPD mass spectrum
K G E R E D L I A Y L K

MH_2^{2+} ×25
b_{11}^{2+}
b_6
b_8
715 716 717

500 600 800 1000 1200 1400 1500
m/z

(e) Fragment ion scan of m/z 454 from the 2D ECD mass spectrum
M I F A G I K K

MH_2^{2+} ×7
c_7

147 400 600 800 1000
m/z

(f) Fragment ion scan of m/z 454 from the 2D IRMPD mass spectrum
M I F A G I K K

MH_2^{2+} ×8
y_6

147 400 600 800 1000
m/z

Figure 2. (a) Horizontal fragment ion scan of m/z 585 corresponding to MH_2^{2+} of TGPNLHGLFGR extracted from the 2D ECD mass spectrum. (b) Horizontal fragment ion scan of m/z 585 corresponding to MH_2^{2+} of TGPNLHGLFGR extracted from the 2D IRMPD mass spectrum. (c) Horizontal fragment ion scan of m/z 718 corresponding to MH_2^{2+} of KGEREDLIAYLK extracted from the 2D ECD mass spectrum. (d) Horizontal fragment ion scan of m/z 718 corresponding to MH_2^{2+} of KGEREDLIAYLK extracted from the 2D IRMPD mass spectrum. (e) Horizontal fragment ion scan of m/z 454 corresponding to MH_2^{2+} of MIFAGIKK extracted from the 2D ECD mass spectrum. (f) Horizontal fragment ion scan of m/z 454 corresponding to MH_2^{2+} of MIFAGIKK extracted from the 2D IRMPD mass spectrum.

charged peptides. In Figure 1c, a harmonic line caused by the nonsinusoidal nature of the precursor ion radius modulation has been highlighted. Its shape is due to an offset by the low frequency of the excitation pulse and the conversion from cyclotron frequencies to mass-to-charge ratios.[17]

Figures 1d and 1e show the autocorrelation lines of the 2D mass spectra with ECD and IRMPD. Because the 2D mass spectra were recorded with transients of 128k data points instead of 4 M data points and because the resolving power on diagonal lines is a combination of the resolving power in the vertical precursor dimension and the resolving power in the horizontal fragment dimension, the resolving power of the autocorrelation line in both 2D mass spectra is R = 14000 at m/z 400 (FWHM: m/z 0.03). Therefore, the peak assignments from the one-dimensional mass spectrum (Figure 1a) are used in order to identify the precursor peaks in the 2D mass spectra.

At m/z 400, the horizontal resolving power of the 2D mass spectrum is R_h = 14000, and the vertical resolving power is R_v = 560. In one-dimensional mass spectrometry, the resolving power measures the number of independent peaks that can be separated in the mass spectrum. In an equivalent manner, in two-dimensional mass spectrometry, this number can be measured by the product of the horizontal and the vertical resolving power. The two-dimensional resolving power at m/z 400 is therefore 7,840,000 (FWHM). As will become apparent, separating the ions in both dimensions expands the scope of the interpretation of the mass spectrometric data.

The resolving power in the 2D mass spectrum is sufficient to separate the precursors in the sample. In this study, mass-to-charge ratios measured in the horizontal fragment dimension of a 2D mass spectrum are given with a 0.01 Da precision. In the vertical precursor dimension, mass-to-charge ratios are given

with a 1 Da precision. The difference in transient length between the one-dimensional mass spectrum and the 2D mass spectra is one of the reasons for the difference in overall signal intensities, since both techniques are based on Fourier transformation. The limitation in transient length is largely imposed by the current computational challenge of processing these large data sets on desktop computers but should be alleviated by moving this computational problem up to cluster computers.

The autocorrelation lines in Figure 1d and 1e show similar peaks with different intensities, both from each other and from the mass spectrum, because of the nature of the 2D FT-ICR experiment. The peaks on the autocorrelation line result from the modulation of the abundance of the precursors remaining after the fragmentation period. The magnitude of the peak on the autocorrelation line depends on the interaction of each precursor ion with the photon or the electron beam. The magnitude of a peak on the autocorrelation line depends both on precursor ion abundance and on how much the signal is depleted by the fragmentation of the precursor.

In the inset on the right side of Figures 1d and 1e, the autocorrelation peaks of MH^+ ion of MIFAGIK at m/z 779.45 are shown. In ECD conditions, the MH^+ ion of MIFAGIK does not produce fragments, but it does capture an electron and neutralize, which causes an ion abundance modulation in the 2D ECD FT-ICR experiment and a high magnitude in the ECD autocorrelation line. In the MS/MS data, with the IRMPD conditions of the 2D FT-ICR experiment, this ion has a fragmentation efficiency of 5%. As a result, the autocorrelation peak has a low magnitude in the IRMPD autocorrelation line. Because the signal for this ion species has a strong constant component, the 2D mass spectrum will show a strong peak at

the maximum m/z ratio (or minimum frequency), with a strong vertical streak caused by scintillation noise (unless the 2D mass spectrum has been denoised).

Figure 2 shows the fragment ion scans of the MH_2^{2+} charge states of three peptides with ECD and IRMPD as fragmentation modes. The internal quadratic calibration of each 2D mass spectrum led to an RMS average of 7.7 ppm mass accuracy for the 2D ECD mass spectrum and 6.3 ppm for the 2D IRMPD mass spectrum.

Figure 2a and Figure 2b show the ECD and IRMPD fragment ion scans of the ion at m/z 585, which corresponds to MH_2^{2+} of peptide TGPNLHGLFGR. The relative abundance of m/z 585 in the one-dimensional mass spectrum is 57% (see Figure 1a and Supporting Information Table S4). The cleavage coverage in the 2D mass spectra is 80% with ECD and 90% with IRMPD. The two mass spectra yield a 100% cleavage coverage for this precursor ion. Complete cleavage coverage can also be obtained in MS/MS (see Supporting Information Table S7). The peak at m/z 585 is not identified in the test chromatogram (see Supporting Information Table S3). Instead, the peptide TGPNLHGLFR is identified by its triply charged state at m/z 390.2. In the one-dimensional mass spectrum, the relative abundance of this peak is 13%. The isotopic distribution of $(TGPNLHGLFR)^{3+}$ overlaps with the isotopic distribution of MH_2^{2+} of tryptic peptide MIFAGIK. The cleavage coverage for $(TGPNLHGLFR)^{3+}$ in the present study was 70% in ECD MS/MS, 0% in the 2D ECD mass spectrum, 100% in IRMPD MS/MS, and 30% in the 2D IRMPD mass spectrum (see Supporting Information Tables S5 and S6). In the test chromatogram, MH_3^{3+} was likely the most abundant charge state for peptide TGPNLHGLFR due to different ionization conditions, and the possibility that this improved the cleavage coverage for this ion cannot be neglected. However, only one charge state of this peptide was fragmented in LC-MS/MS, whereas all charge states were fragmented in the 2D mass spectrum. This enhances the cleavage coverage of the peptide.

The fragment ion scans of m/z 718 from the 2D ECD mass spectrum and the 2D IRMPD mass spectrum are shown in Figure 2c and 2d. In the mass spectrum (see Figure 1a), this peak is identified as MH_2^{2+} of peptide GEREDLIAYLKK in the test chromatogram. The relative abundance of this peak in the one-dimensional mass spectrum is 11% (see Supporting Information Table S4). In Figures 2c and 2d, two peaks can be assigned to fragments of GEREDLIAYLKK: c_{11} at m/z 1305.70 (-15 ppm) in Figure 2c and b_{11}^{2+} at m/z 644.85 (1.81 ppm) in Figure 2d. However, these fragments can also be products of the dissociation of MH_2^{2+} of KGEREDLIAYLK. Several other peaks in the fragment ion scans can also be assigned to fragments of KGEREDLIAYLK but not GERED-LIAYLKK: c_{10} at m/z 1992.64 (-0.36 ppm) in Figure 2a and b_6 at m/z 715.34 (15.6 ppm) in Figure 2d.[32] As a result, this peptide can be consistently assigned as KGEREDLIAYLK. This result is consistent with the data obtained in MS/MS spectra (see Supporting Information Tables S5 and S6).

Figure 2e and 2f show the horizontal fragment ion scans for the ion at m/z 454, which corresponds to MH_2^{2+} from the peptide fragment MIFAGIKK, extracted from the 2D ECD mass spectrum (Figure 2e) and the 2D IRMPD mass spectrum (Figure 2f). MIFAGIKK is not identified in the chromatogram and has not been analyzed in MS/MS because of its low abundance and because of its absence in the test chromatogram (see Supporting Information Table S3). In the mass spectrum

of the tryptic digest of cytochrome c (see Figure 1a), the relative abundance of MH_2^{2+} of MIFAGIKK is 2.3%. In the autocorrelation line of the 2D ECD mass spectrum (see Figure 1c), its relative abundance is 2.5% (ion at maximum abundance: m/z 728.85). In the autocorrelation line of the 2D IRMPD mass spectrum (see Figure 1b), its relative abundance is 1.4% (ion at maximum abundance: m/z 728.85).

By combining both fragment ion scans for m/z 454, two fragments of $(MIFAGIKK)^{2+}$ can be assigned, which corresponds to a 25% cleavage coverage for this low abundance peptide. In direct infusion MS/MS, this result could not have been achieved without extensive external ion accumulation (several seconds) and accumulating spectra over several hundred transients in order to get a comparable signal-to-noise ratio for the MS/MS data and the same sequence coverage. With 2D mass spectrometry, the fragmentation of this peptide ion has been conducted simultaneously with all other ions and brings additional information to the analysis of the sample.

Figure 3 shows the ECD fragmentation pattern of the ion at m/z 545, both as MS/MS data (Figure 3a) and as a fragment ion scan from the 2D mass spectrum (Figure 3b). Both the MS/MS data and the fragment ion scans presented in Figure 3
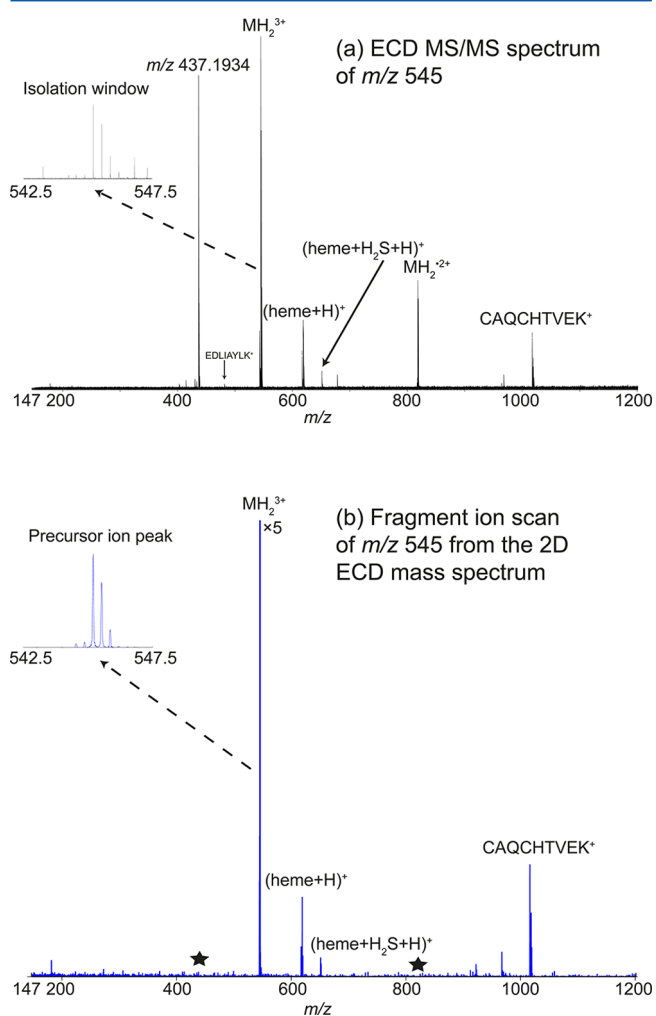

Figure 3. (a) MS/MS data of m/z 545 corresponding to MH_2^{3+} of [CAQCHTVEK+heme]. (b) Horizontal fragment ion scan of m/z 545 corresponding to MH_2^{3+} of [CAQCHTVEK+heme] extracted from the 2D ECD mass spectrum.

agree with the assignment of (CAQCHTVEK+heme), as the precursor primarily dissociates into CAQCHTVEK$^+$ and heme$^+$ or into [CAQCHTVEK-2H]$^+$ and [heme+2H]$^+$. There are several differences between the ECD MS/MS data and the fragment ion scan. In the MS/MS data, the quadrupolar isolation window is set at ±2.5 Da at m/z 545 in order to optimize the abundance of the precursor. All ions with m/z ratios within that window are present in the ICR cell before fragmentation, which lessens the correlation between precursors and fragments. In the fragment ion scan, however, the window containing precursors is much narrower, with resolution in the precursor ion dimension of about 1.5 Da. Furthermore, two peaks are present in the MS/MS data and are not present in the fragment ion scan from the 2D mass spectrum. The most intense one is at m/z 437.1934 and can be recognized as the sodiated contaminant from the solvent (assigned in the one-dimensional mass spectrum as $C_{24}H_{30}O_6Na^+$). The presence of this peak is most likely due to ineffective isolation in the quadrupole. The other peak that is present in the MS/MS data but not in the fragment ion scan is the peak at m/z 817.8143 corresponding to $MH_2^{2\bullet+}$. However, this peak is present in the raw (without denoising) 2D mass spectrum (see Figure S1 in the Supporting Information). Its absence is an artifact of the urQRd rank being too low, which leads to the disappearance of low-magnitude peaks in the vertical precursor ion dimension. In the vertical dimension, the $MH_2^{2\bullet+}$ ion resulting from the capture of one electron by MH_2^{3+} is in the same column as the ^{13}C isotope of MH_2+ precursor species of (CAQCHTVEK+heme) and has a much lower abundance peak. Denoising with a small urQRd rank has deleted the peak corresponding to $MH_2^{2\bullet+}$ ion resulting from the capture of one electron by MH_2^{3+}. No peptide backbone cleavages are observed in either spectra, in agreement with the hypothesis that the electron is captured by the heme.[37] Figure 4 shows zoom-ins of various areas in the ECD MS/MS data and the fragment ion scan extracted from the 2D ECD mass spectrum of the ion observed at m/z 545. A zoom-in of the areas between m/z 616−622 (Figures 4a for the MS/MS data and 4d for the 2D mass spectrum) shows the peaks of heme$^+$ and [heme+2H]$^+$. A zoom-in of the areas between m/z 1015−1021 (Figures 4f for the MS/MS data and 4I for the 2D mass spectrum) shows [CAQCHTVEK-2H]$^+$ and CAQCHTVEK$^+$. The isotopic distributions of heme$^+$ and [heme+2H]$^+$ overlap, as do the isotopic distributions of [CAQCHTVEK-2H]$^+$ and CAQCHTVEK$^+$. The isotopic pattern simulations of heme$^+$ (Figure 4b), [heme+2H]$^+$ (Figure 4c), [CAQCHTVEK-2H]$^+$ (Figure 4g), and CAQCHTVEK$^+$ (Figure 4h) show that there is indeed an overlap between two ion species in both regions. The other fragment that is observed is [heme+H$_2$S]$^+$, but [CAQCHTVEK-H$_2$S]$^+$ is not observed.

The ion intensities between the MS/MS data and the fragment ion scan are well correlated, which is apparent in Figures 4f and 4i between the isotopic distributions of [CAQCHTVEK-2H]$^+$ and CAQCHTVEK$^+$. In a zoom-in of the 2D mass spectrum for these fragment ion peaks (Figure 4j), the monoisotopic fragments are clearly produced by the monoisotopic precursor ion, and the ^{13}C isotopic fragments are mostly produced by the ^{13}C isotope of the precursor. In the zoom-ins of the MS/MS data and the fragment ion scan for the m/z 616−622 region (Figures 4a and 4d), there is a discrepancy between the relative abundances of the most abundant isotopologue of the heme$^+$ fragment ($^{12}C_{34}H_{33}N_4O_4Fe^+$ at m/z 617.1846) and the second most
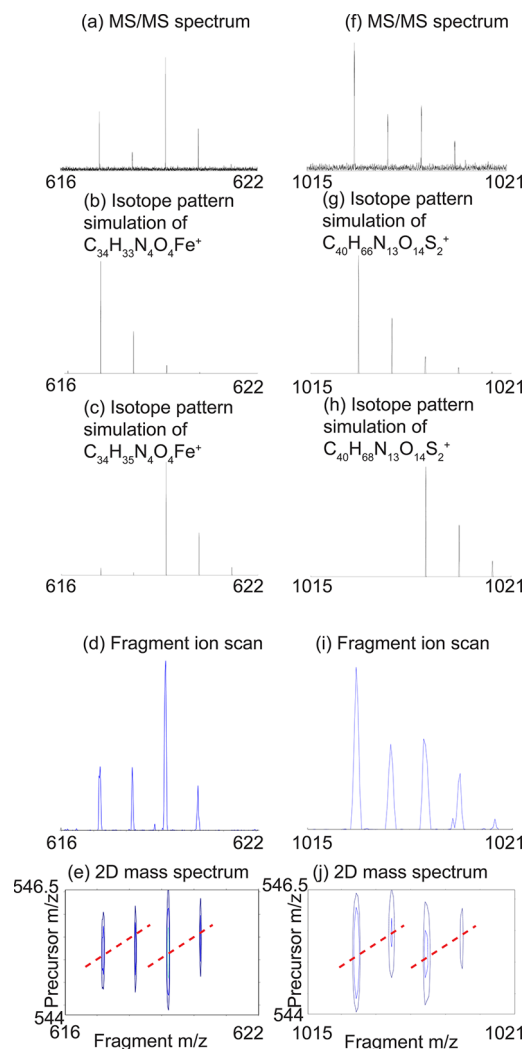

Figure 4. (a) Zoom on the (heme)$^+$ fragment in the MS/MS data. (b) Simulation of the isotopic pattern of $C_{34}H_{33}N_4O_4Fe^+$. (c) Simulation of the isotopic pattern of $C_{34}H_{35}N_4O_4Fe^+$. (d) Zoom on the (heme)$^+$ fragment in the fragment ion scan of m/z 545 in the 2D ECD mass spectrum. (e) Zoom on the (heme)$^+$ fragment in the 2D ECD mass spectrum. (f) Zoom on the [CAQCHTVEK]$^+$ fragment in the MS/MS data. (g) Simulation of the isotopic pattern of $C_{40}H_{66}N_{13}O_{14}S_2^+$. (h) Simulation of the isotopic pattern of $C_{40}H_{68}N_{13}O_{14}S_2^+$. (i) Zoom on the [CAQCHTVEK]$^+$ fragment in the fragment ion scan of m/z 545 in the 2D ECD mass spectrum. (j) Zoom on the [CAQCHTVEK]$^+$ fragment in the 2D ECD mass spectrum.

abundant isotopologue ($^{13}C^{12}C_{33}H_{33}N_4O_4Fe^+$ at m/z 618.1878). The zoom-in of the 2D mass spectrum shows that both isotopologues are produced from the same precursor isotopologue containing only ^{12}C. The isotopic pattern of Fe, containing 5.8% of ^{54}Fe, 91.8% of ^{56}Fe, 2.1% of ^{57}Fe, and 0.3% of ^{58}Fe, has no incidence on the two-dimensional isotopic distribution of the heme ions because it contains only one Fe atom. As a result, the peak at m/z 618.19 in the 2D mass spectrum can be identified as the overlap of the peak corresponding to $^{13}C^{12}C_{33}H_{33}N_4O_4Fe^+$ (m/z 618.187840) and of the peak corresponding to $^{12}C_{34}H_{34}N_4O_4Fe^{\bullet+}$ (m/z 618.195665). The difference in mass-to-charge ratio between these two ions is m/z 0.007825, which requires a minimum resolving power of 80,000 at m/z 618. Although the resolving power in the 2D mass spectrum is not sufficient to separate these two peaks, both fragments can still be identified thanks to

the second dimension. The peak for $C_{34}H_{34}N_4O_4Fe^{\bullet+}$ could not be found in the MS/MS data for m/z 545, because the fragmentation conditions are different from those in the 2D mass spectrum (ECD irradiation of 0.05 s in the MS/MS data and 0.1 s in the 2D mass spectrum).

Two tryptic peptide ions in the mass spectrum (see Figure 1a) are separated by 0.0156 Da/e: MH_3^{3+} of TGPNLHGLFGR (m/z 390.2122) and MH_2^{2+} of MIFAGIK (m/z 390.2278). In one-dimensional MS/MS, the resolving power necessary to separate these two ions is 25000. This isolation is extremely difficult to achieve with quadrupole isolation. Other in-cell isolation techniques have been shown to successfully isolate ions with enough resolving power: Stored Waveform Inverse Fourier Transform (SWIFT) has achieved ion isolation with a resolving power of 29000,[38] single frequency excitation has achieved isolation with a resolving power of 50000,[39] and Correlated Harmonic Excitation Fields (CHEF) has achieved a resolving power of 60000.[40] However, these methods required significant tuning of the experimental parameters and correlating precursors, and fragments of very close mass-to-charge ratios remain difficult in one-dimensional MS/MS, because of the near-resonant excitation of the neighboring peaks,[41] resulting in the need for very accurate, long duration, low power excitation pulses.

In the interpretation of a 2D mass spectrum, advantage can be taken from the different charge state between the two ion species and the isotopic distribution of the fragment ion peaks, as can be seen in Figure 5. When a precursor of charge n fragments by loss of charge p and mass $m_{neutral}$, the equation of the dissociation line is

$$(m/z)_{precursor} = \frac{n-p}{n}(m/z)_{fragment} + \frac{m_{neutral}}{n} \qquad (1)$$

in which $(m/z)_{precursor}$ is the m/z ratio of the precursor ion and $(m/z)_{fragment}$ is the m/z ratio of the fragment ion. For small peptides, the isotopic distribution of the fragment ion follows this line in the 2D mass spectrum.
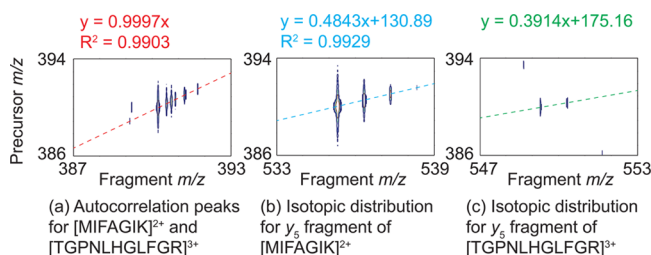

Figure 5. (a) Zoom on the autocorrelation peaks for $[MIFAGIK]^{2+}$ and $[TGPNLHGLFGR]^{3+}$ at m/z 390 in the 2D IRMPD mass spectrum. (b) Zoom on the fragment ion peaks for the y_5 fragment of $[MIFAGIK]^{2+}$ in the 2D IRMPD mass spectrum. (c) Zoom on the fragment ion peaks for the y_5 fragment of $[TGPNLHGLFGR]^{3+}$ in the 2D IRMPD mass spectrum.

Figure 5a shows the autocorrelation peaks of $MIFAGIK^{2+}$ (m/z 390.23) and $TGPNLHGLFGR^{3+}$ (m/z 390.21) in the 2D IRMPD mass spectrum. The horizontal resolving power of the monoisotopic peak is 12200 (FWHM = 0.032), and the vertical resolving power is 580 (FWHM = 0.67). The two precursor peaks cannot be resolved. However, the use of the isotopic distribution of the fragment peaks leads to accurate correlation between precursor and fragment. Figure 5b shows the isotopic distribution of a fragment of either $MIFAGIK^{2+}$ or TGPNL-

$HGLFGR^{3+}$ in the 2D IRMPD mass spectrum at $(m/z)_{fragment}$ 535.32. The trendline for the isotopic distribution has a slope of 0.48 (approximately 0.5). With eq 1, the charge of the precursor can therefore be calculated as $n = 2$. The mass of the lost moiety is 262 Da, which corresponds to the mass of MI. This fragment can be assigned as y_5 of $MIFAGIK^{2+}$. In Figure 5c, only two isotopes of the fragment at m/z 549.31 are intense enough to be seen in the 2D mass spectrum, which makes the information contained in the trendline equation less accurate. However, the slope of 0.3914 is close enough to 1/3 in order to assign the precursor ion as a triply charged ion with eq 1. The fragment ion can be assigned as y_5 of $TGPNLHGLFGR^{3+}$.

A Comparison between the Standard MS/MS Analysis and the 2D FT-ICR MS Proteomics Experiment. When the results from both ECD and IRMPD were combined, the cleavage coverage with MS/MS was 67%, and the cleavage coverage of the 2D mass spectra was 63%. Transients for 2D FT-ICR experiments are shorter than transients for MS/MS experiments, because data files for 2D FT-ICR MS are very large (3 GB); so transient size is restricted for practical processing reasons. Increasing the length of transients in the 2D FT-ICR experiment will increase the sensitivity and the resolution of the technique and therefore will also increase the cleavage coverage of proteins in bottom-up proteomics. Other advantages of 2D FT-ICR MS over MS/MS and LC-MS/MS are that 2D mass spectra show the fragmentation patterns of all charge states of each peptide, thereby increasing cleavage coverage. 2D mass spectra also show the fragmentation patterns of more ion species than LC-MS/MS. Furthermore, while recording a 2D mass spectrum takes the same amount of experimental time and sample regardless of the complexity of the sample, in MS/MS experimental time and sample consumption is proportional to the complexity of the sample. A more detailed comparison between 2D FT-ICR MS analysis and MS/MS can be found in the Supporting Information.

■ CONCLUSION

This tryptic digest is one of the first to be published in-depth in 2D FT-ICR mass spectrometry,[42] with two experiments that lasted 20 min each. For peptides of high and low abundance, the fragmentation pattern for all ions was recorded, including sodium or potassium adducts.

The differences between the mass spectrum and the two autocorrelation lines show that conflating the two kinds of spectras can lead to misinterpretation of the data. Precursor ions that are not affected by the fragmentation conditions of the 2D FT-ICR experiment only show a small peak in the autocorrelation line, but the scintillation noise caused by random fluctuations of their abundance during the experiment can lead to spurious peaks in fragment ion scans, which can lead to additional misinterpretation. Denoising 2D mass spectra with the urQRd algorithm can significantly reduce this problem but does not eliminate it.[16]

Precursor ion resolution in a 2D experiment is controlled by the number of steps chosen in the pulse sequence, so it can be increased arbitrarily with a concomitant increase in total experimental duration and computing time. Combined with the urQRd denoising algorithm, this leads to fragmentation patterns with fewer spurious peaks and a high confidence in fragment peak assignments. By using the slopes of line along the isotopic distributions of fragment ions, fragments can be accurately correlated with their precursors in cases where the

precursor ions have the same nominal mass but different charge states.

2D FT-ICR mass spectrometry can be used for bottom-up protein analysis. Peak lists could be generated from 2D mass spectra and used to search against proteomics databases for peptide and protein identification. The fact that 2D mass spectra contain the fragmentation patterns of peptides at different charge states can improve cleavage coverage. 2D FT-ICR MS can be applied to digests of proteins of higher mass or mixtures of proteins, as well as intact proteins in top-down proteomics.

■ ASSOCIATED CONTENT

ⓢ Supporting Information

The Supporting Information is available free of charge on the ACS Publications website at DOI: 10.1021/acs.analchem.5b04878.

> Detailed principle of 2D FT-ICR MS, Detailed experimental methods, Experimental conditions for MS/MS spectra using ECD and using IRMPD as a fragmentation mode, List of peptides in the test chromatogram provided by Thermo Scientific for the tryptic digest of cytochrome c, Peak assignments of the mass spectrum of the tryptic digest of cytochrome c, List of fragments identified in the MS/MS data and the 2D mass spectrum with ECD as a fragmentation mode and with IRMPD as a fragmentation mode, Peak assignments for additional MS/MS spectra for m/z 584, Horizontal fragment ion scan of m/z 545 corresponding to MH_2^{3+} of (CAQCHTVEK+heme) extracted from the 2D ECD mass spectrum prior to urQRd denoising, Peaks caused by scintillation noise are indicated with a star, Horizontal fragment ion scan from the 2D IRMPD mass spectrum of m/z 415.2 and of m/z 432.2, Fragment ion peaks of the precursor ion at m/z 415.2 and at m/z 432.2 extracted from the 2D IRMPD mass spectrum, Detailed comparison between MS/MS analysis and 2D FT-ICR analysis of cytochrome c tryptic digest (PDF)

■ AUTHOR INFORMATION

Corresponding Author

*Phone: 44 (0) 2476 151 008. Fax: 44 (0) 2476 151 009. E-mail: p.oconnor@warwick.ac.uk.

Present Address

¶(M.-A.C.) DataStorm, 60 rue Etienne Dolet - 92240 Malakoff France.

Author Contributions

The manuscript was written through contributions of all authors. All authors have given approval to the final version of the manuscript. All authors contributed equally.

Notes

The authors declare no competing financial interest.

■ ACKNOWLEDGMENTS

■ ABBREVIATIONS

FT-ICR MS	Fourier transform ion cyclotron resonance mass spectrometry
MS/MS	tandem mass spectrometry
2D FT-ICR MS	two-dimensional Fourier transform ion cyclotron resonance mass spectrometry
IRMPD	infrared multiphoton dissociation
ECD	electron capture dissociation

■ REFERENCES

(1) Comisarow, M. B.; Marshall, A. G. *Chem. Phys. Lett.* **1974**, *26*, 489−490.

(2) Comisarow, M. B.; Marshall, A. G. *Chem. Phys. Lett.* **1974**, *25*, 282−283.

(3) Pfaendler, P.; Bodenhausen, G.; Rapin, J.; Houriet, R.; Gäumann, T. *Chem. Phys. Lett.* **1987**, *138*, 195−200.

(4) Kumar, A.; Ernst, R. R.; Wuethrich, K. *Biochem. Biophys. Res. Commun.* **1980**, *95*, 1−6.

(5) Marshall, A. G.; Wang, T. C. L.; Ricca, T. L. *Chem. Phys. Lett.* **1984**, *105*, 233−236.

(6) Guan, S.; Jones, P. R. *J. Chem. Phys.* **1989**, *91*, 5291−5295.

(7) van Agthoven, M. A.; Delsuc, M.-A.; Bodenhausen, G.; Rolando, C. *Anal. Bioanal. Chem.* **2013**, *405*, 51−61.

(8) Pfaendler, P.; Bodenhausen, G.; Rapin, J.; Walser, M. E.; Gäumann, T. *J. Am. Chem. Soc.* **1988**, *110*, 5625−5628.

(9) Bensimon, M.; Zhao, G.; Gäumann, T. *Chem. Phys. Lett.* **1989**, *157*, 97−100.

(10) Ross, C. W., III; Guan, S.; Grosshans, P. B.; Ricca, T. L.; Marshall, A. G. *J. Am. Chem. Soc.* **1993**, *115*, 7854−7861.

(11) van der Rest, G.; Marshall, A. G. *Int. J. Mass Spectrom.* **2001**, *210-211*, 101−111.

(12) van Agthoven, M. A.; Delsuc, M.-A.; Rolando, C. *Int. J. Mass Spectrom.* **2011**, *306*, 196−203.

(13) van Agthoven, M. A.; Chiron, L.; Coutouly, M.-A.; Delsuc, M.-A.; Rolando, C. *Anal. Chem.* **2012**, *84*, 5589−5595.

(14) Delsuc, M. A. https://bitbucket.org/delsuc/spike (accessed July 13, 2015).

(15) van Agthoven, M. A.; Coutouly, M.-A.; Rolando, C.; Delsuc, M.-A. *Rapid Commun. Mass Spectrom.* **2011**, *25*, 1609−1616.

(16) Chiron, L.; van Agthoven, M. A.; Kieffer, B.; Rolando, C.; Delsuc, M.-A. *Proc. Natl. Acad. Sci. U. S. A.* **2014**, *111*, 1385−1390.

(17) van Agthoven, M. A.; Chiron, L.; Coutouly, M.-A.; Sehgal, A. A.; Pelupessy, P.; Delsuc, M.-A.; Rolando, C. *Int. J. Mass Spectrom.* **2014**, *370*, 114−124.

(18) van Agthoven, M.; Barrow, M.; Chiron, L.; Coutouly, M.-A.; Kilgour, D.; Wootton, C.; Wei, J.; Soulby, A.; Delsuc, M.-A.; Rolando, C.; O'Connor, P. *J. Am. Soc. Mass Spectrom.* **2015**, *26*, 2105−2114.

(19) Yates, J. R., III; Speicher, S.; Griffin, P. R.; Hunkapiller, T. *Anal. Biochem.* **1993**, *214*, 397−408.

(20) Zhang, Z.; Smith, D. L. *Protein Sci.* **1993**, *2*, 522−531.

(21) Chen, W.-Y.; Chen, Y.-C. *Anal. Bioanal. Chem.* **2006**, *386*, 699−704.

(22) Caravatti, P.; Allemann, M. *Org. Mass Spectrom.* **1991**, *26*, 514−518.

(23) Tsybin, Y. O.; Witt, M.; Baykut, G.; Kjeldsen, F.; Hakansson, P. *Rapid Commun. Mass Spectrom.* **2003**, *17*, 1759−1768.

(24) Qi, Y.; Thompson, C. J.; Van Orden, S. L.; O'Connor, P. B. *J. Am. Soc. Mass Spectrom.* **2011**, *22*, 138−147.

(25) Qi, Y.; Barrow, M. P.; Van Orden, S. L.; Thompson, C. J.; Li, H.; Perez-Hurtado, P.; O'Connor, P. B. *Anal. Chem.* **2011**, *83*, 8477−8483.

(26) Qi, Y.; Barrow, M. P.; Li, H.; Meier, J. E.; Van Orden, S. L.; Thompson, C. J.; O'Connor, P. B. *Anal. Chem.* **2012**, *84*, 2923−2929.

(27) Qi, Y.; Witt, M.; Jertz, R.; Baykut, G.; Barrow, M. P.; Nikolaev, E. N.; O'Connor, P. B. *Rapid Commun. Mass Spectrom.* **2012**, *26*, 2021−2026.

(28) Qi, Y.; Li, H.; Wills, R. H.; Perez-Hurtado, P.; Yu, X.; Kilgour, D. P. A.; Barrow, M. P.; Lin, C.; O'Connor, P. B. *J. Am. Soc. Mass Spectrom.* **2013**, *24*, 828−834.

(29) Kilgour, D.; Wills, R.; Qi, Y.; O'Connor, P. *Anal. Chem.* **2013**, *85*, 3903−3911.

(30) Kilgour, D.; Neal, M.; Soulby, A.; O'Connor, P. *Rapid Commun. Mass Spectrom.* **2013**, *27*, 1977−1982.

(31) Francl, T. J.; Sherman, M. G.; Hunter, R. L.; Locke, M. J.; Bowers, W. D.; McIver, R. T., Jr. *Int. J. Mass Spectrom. Ion Processes* **1983**, *54*, 189−199.

(32) Ledford, E. B., Jr.; Rempel, D. L.; Gross, M. L. *Anal. Chem.* **1984**, *56*, 2744−2748.

(33) Licklider, L.; Wang, X.-Q.; Desai, A.; Tai, Y.-C.; Lee, T. D. *Anal. Chem.* **2000**, *72*, 367−375.

(34) Keough, T.; Lacey, M. P.; Youngquist, R. S. *Rapid Commun. Mass Spectrom.* **2000**, *14*, 2348−2356.

(35) Russell, D. H.; Edmondson, R. D. *J. Mass Spectrom.* **1997**, *32*, 263−276.

(36) Henderson, S. C.; Valentine, S. J.; Counterman, A. E.; Clemmer, D. E. *Anal. Chem.* **1999**, *71*, 291−301.

(37) Zubarev, R. A.; Horn, D. M.; Fridriksson, E. K.; Kelleher, N. L.; Kruger, N. A.; Lewis, M. A.; Carpenter, B. K.; McLafferty, F. W. *Anal. Chem.* **2000**, *72*, 563−573.

(38) O'Connor, P. B.; McLafferty, F. W. *J. Am. Soc. Mass Spectrom.* **1995**, *6*, 533−535.

(39) Heck, A. J. R.; De Koning, L. J.; Pinkse, F. A.; Nibbering, N. M. M. *Rapid Commun. Mass Spectrom.* **1991**, *5*, 406−414.

(40) de Koning, L. J.; Nibbering, N. M. M.; van Orden, S. L.; Laukien, F. H. *Int. J. Mass Spectrom. Ion Processes* **1997**, *165-166*, 209−219.

(41) Senko, M. W.; Speir, J. P.; McLafferty, F. W. *Anal. Chem.* **1994**, *66*, 2801−2808.

(42) Simon, H. J.; van Agthoven, M. A.; Lam, P. Y.; Floris, F.; Chiron, L.; Delsuc, M. A.; Rolando, C.; Barrow, M. P.; O'Connor, P. B. *Analyst* **2016**, *141*, 157−165.